

Electron Acceleration in 3D Magnetic Reconnection

J. T. Dahlin, J. F. Drake,* and M. Swisdak

*Institute for Research in Electronics and Applied Physics,
University of Maryland, College Park, Maryland 20742, USA*

(Dated: March 14, 2019)

Abstract

A kinetic simulation of 3D collisionless magnetic reconnection shows a dramatic enhancement of electron acceleration when compared with a 2D system. In the 2D system, electrons are trapped in magnetic islands which limits their energy gain, whereas in the 3D system the stochastic magnetic field enables the electrons to access volume-filling acceleration regions. The dominant accelerator of the most energetic electrons is a Fermi mechanism associated with reflection of charged particles from contracting field lines.

Magnetic reconnection is a ubiquitous plasma process that converts magnetic energy into thermal and kinetic energy. Of particular interest is the production of non-thermal particles, in which a fraction of the plasma population is driven to energies much larger than that found in the ambient medium. Reconnection is thought to be an important driver of such particles in phenomena such as gamma ray bursts [1, 2], stellar and solar flares [3], and magnetospheric storms [4]. Recent observations of solar flares reveal the remarkable efficiency of electron acceleration: a large fraction of the electrons in the flaring region become a part of the nonthermal spectrum, with a resulting energy content comparable to that of the magnetic field [5, 6].

Mechanisms for particle acceleration have been explored and compared in a variety of papers, e.g. [7–12]. Several authors [9, 13, 14] have examined acceleration by electric fields parallel to the local magnetic field (E_{\parallel}). However, parallel electric fields are typically localized near reconnection X-lines and separatrices, which limits the number of electrons that can be accelerated through this mechanism.

Drake et al. [15] proposed a mechanism whereby charged particles gain energy as they reflect from the ends of contracting magnetic islands, a process analogous to the first-order Fermi acceleration of cosmic rays. This mechanism operates wherever there are contracting field lines in a reconnection region, and therefore develops during single X-line reconnection or as magnetic islands merge [12, 15–17]. This mechanism is therefore volume filling and can accelerate large number of particles.

In a recent article [18], we developed a method for calculating the total acceleration due to three fundamental mechanisms: parallel electric fields E_{\parallel} , betatron acceleration associated with conservation of the magnetic moment, and Fermi reflection due to the relaxation of curved magnetic field lines. We found that Fermi reflection dominated in reconnection where the magnetic fields are roughly antiparallel (a result also found in [19]). However, in guide field reconnection (which includes a magnetic field component perpendicular to the plane of the simulation) where the current layers around the X-line and associated regions

where $E_{\parallel} \neq 0$ are longer, Fermi reflection and E_{\parallel} were both important drivers of particle acceleration. We also showed that E_{\parallel} is primarily localized to the small region near the X-line, whereas the Fermi reflection term is distributed throughout a large region at the ends of the islands. However, we did not address the scaling of each mechanism with particle energy. This is important for determining the mechanism responsible for producing the most energetic particles.

Studies of particle acceleration in reconnection have primarily been based on 2D simulations, which exhibit some disparities when compared to reconnection observations. For example, while energetic particles are typically confined to narrow boundary layers in 2D simulations [20], Wind spacecraft observations of magnetotail reconnection found these particles to be distributed throughout the reconnecting region [4].

Two-dimensional simulations impose limitations on the magnetic topology as well as the available spectrum of instabilities. Reconnection in 3D systems becomes turbulent as a result of the generation of magnetic islands along separatrices and adjacent surfaces [21, 22]. While test particle trajectories in MHD fields have been used to explore acceleration mechanisms, [23, 24] the absence of feedback of energetic particles on the reconnection process in such models limits their applicability to real systems. Recent 3D studies of kinetic reconnection examined particle acceleration in simulations of electron-positron plasmas [19, 25]. However, these studies focused on relativistic regimes where the magnetic energy per particle exceeds the rest mass energy. Additionally, these simulations had no asymptotic guide field, an important parameter in many astrophysical regimes. Hence, the impact of complex 3D magnetic fields on particle acceleration remains an open topic.

Here, we explore magnetic reconnection in a 3D system with a strong guide field. We find that the efficiency of particle acceleration is greatly increased compared to that in a 2D system. We show that this occurs because the complex 3D magnetic fields enable the most energetic particles to access volume-filling acceleration sites rather than being confined to a single magnetic island which no longer accelerates particles once it has fully contracted. We also examine the energy dependence of the dominant E_{\parallel} and Fermi acceleration mechanisms, and find that Fermi reflection is the primary accelerator of the energetic electrons.

We explore particle acceleration via simulations using the massively parallel 3D particle-in-cell (PIC) code `p3d` [26]. Particle trajectories are calculated using the relativistic Newton-Lorentz equations, and the electromagnetic fields are advanced using Maxwell's equations. In

this paper, we examine a 3D simulation with dimensions $L_x \times L_y \times L_z = 51.2d_i \times 25.6d_i \times 25.6d_i$ and an analogous 2D simulation with $L_x \times L_y = 51.2d_i \times 25.6d_i$, where $d_i = c/\omega_{pi}$ is the ion skin depth. The initial condition consists of two force-free current sheets, each with a magnetic field of the following form:

$$B_x = B_0 \tanh\left(\frac{y - y_0}{w_0}\right)$$

$$B_z = B_0 \sqrt{2 - B_x^2/B_0^2}$$

where B_0 is the asymptotic reconnecting field, y_0 is the center of the current sheet and $w_0 = 0.25d_i$ is the half-width. The initial electron and proton temperatures are $T_e = T_i = 0.25m_i c_A^2$, and the initial density n_0 and pressure p are constant so that $\beta = 8\pi p/B^2 = 0.5$. We use an artificial proton to electron mass ratio $m_i/m_e = 25$, and the speed of light is $c = 15c_A$, where $c_A = B_0/\sqrt{4\pi m_i n_0}$. Time is normalized to the proton cyclotron time $\Omega_{ci}^{-1} = m_i c/eB$.

Reconnection develops from particle noise via the tearing instability, generating interacting flux ropes which grow and merge until they reach the system size at $t\Omega_{ci} \sim 60$. Fig. 1 shows an isosurface of one component of the electron current density J_{ez} at $t\Omega_{ci} = 50$ in the 3D simulation. The current exhibits filamentary structure which develops from instabilities with $k_z \neq 0$ that are prohibited in 2D reconnection simulations [22].

Energy spectra (top panel of Fig. 2) reveal significant electron acceleration in both simulations. However, the 3D simulation produces a greater number of energetic particles: the fraction of electrons with energy exceeding $0.5m_e c^2$ is roughly an order of magnitude larger than in the 2D simulation. By comparison, there is little difference in the thermal component of the spectra, and the total magnetic energy dissipation (not shown) is comparable in the two simulations. This suggests that the increased energetic electron production in the 3D system is due to enhanced acceleration efficiency rather than an increase in the total energy imparted to the electrons.

The spatial distribution of the most energetic particles (shown in the left-hand panels of Fig. 3) also differs between these simulations: these particles occupy narrow bands well inside the islands in the 2D simulation, but are distributed throughout the reconnecting region in the 3D simulation. In the 2D system, the reconnected field lines form closed loops (islands) which trap particles. The stochastic structure of the magnetic field in the 3D system, however, allows field-line-following particles to wander throughout the chaotic

reconnecting region [27]. The distribution of the energetic particles in the 3D simulation is broadly consistent with Wind magnetotail observations where energetic electrons are seen for more than an hour and therefore must occupy a large region [4].

In order to examine the mechanisms responsible for accelerating these particles, we assume a guiding-center approximation relevant for a strong guide field [28]. In this limit, the evolution of the kinetic energy ϵ of a single electron can be written as:

$$\frac{d\epsilon}{dt} = qE_{\parallel}v_{\parallel} + \frac{\mu}{\gamma} \left(\frac{\partial B}{\partial t} + \mathbf{u}_E \cdot \nabla B \right) + \gamma m_e v_{\parallel}^2 (\mathbf{u}_E \cdot \boldsymbol{\kappa}) \quad (1)$$

where $E_{\parallel} = \mathbf{E} \cdot \mathbf{b}$ is the parallel electric field, $\mu = m_e \gamma^2 v_{\perp}^2 / 2B$ is the magnetic moment, \mathbf{u}_E is the $\mathbf{E} \times \mathbf{B}$ velocity corresponding to the advection of the magnetic field, and $\boldsymbol{\kappa} = \mathbf{b} \cdot \nabla \mathbf{b}$ is the magnetic curvature. The velocity components parallel and perpendicular to the magnetic field are v_{\parallel} and v_{\perp} , respectively; γ is the relativistic Lorentz factor, and \mathbf{b} is the unit vector in the direction of the local magnetic field.

The first term on the right-hand-side of the equation corresponds to acceleration by parallel electric fields, which are typically localized near the reconnection X-line and along separatrices. The second term corresponds to betatron acceleration and is a consequence of the conservation of the magnetic moment μ : when a particle experiences a change in B , its perpendicular energy evolves to compensate. In the case of reconnection, which reduces the overall magnetic field, betatron acceleration typically reduces particle energy [18]. The last term corresponds to reflection of particles from contracting magnetic field lines, a type of first order Fermi acceleration [15, 16]. This occurs where tension is released as magnetic fields advect in the direction of magnetic curvature ($\mathbf{u}_E \cdot \boldsymbol{\kappa} > 0$).

Equation 1 reveals that the acceleration mechanisms have different scaling with the particle energy: the Fermi reflection term is second order in the parallel velocity, whereas the parallel electric field term is only first order. The bottom panel of Fig. 2 shows the average acceleration per particle for both E_{\parallel} and Fermi reflection in the 3D simulation at $t\Omega_{ci} = 50$. The bulk thermal electrons (low energies) are primarily accelerated by E_{\parallel} , whereas Fermi reflection is more important at high energies. This indicates that Fermi reflection is the dominant accelerator of the most energetic particles, consistent with the energy scaling of Eq. 1.

The Fermi reflection term for the most energetic electrons ($> 0.5m_e c^2$) is shown on the right-hand side of Fig. 3. While acceleration occurs throughout the reconnection exhaust

in the 3D simulation, in 2D the acceleration is limited to narrow bands near the cores of magnetic islands. This contrast suggests that the stochastic 3D field structure allows the electrons to have greater access to the acceleration regions where magnetic energy is being released.

To explore the reason for enhanced acceleration in the 3D system, we examine the trajectories of the 750 most energetic electrons in each simulation. A sample trajectory from the 2D simulation is shown in the top left panel in Fig. 4. The electron begins in the tail of the electron distribution with kinetic energy $\epsilon \approx 0.4m_e c^2$. The electron streams along a field line outside the reconnection region before accelerating at an X-line near $x \sim 50$ and becoming trapped in an island. The electron bounces several times inside this island, accelerating up to $\epsilon \approx 0.8m_e c^2$. By this point, the field line the electron is following has released its tension, so acceleration ceases even as the electron continues to bounce.

The top right panel of Fig. 4 shows a sample electron trajectory from the 3D simulation. The electron is not confined to any single island, but instead moves relatively freely throughout the domain. This allows it to undergo significantly greater acceleration than the electron from the 2D simulation, as it is able to return to active acceleration regions rather than being confined to the stagnant field lines near island cores. The acceleration of this particle is spread across a number of different islands, enabling it to reach a maximum energy of $\epsilon \approx 1.15m_e c^2$. The Supplemental Material [29] includes videos of both particle trajectories in the time evolving field of the simulation.

The electron trajectories shown here are relatively generic for their respective simulations. Though the acceleration details differ, all of the electrons in the 2D simulation are confined to single islands, whereas no electrons in the 3D show significant trapping. The bottom panels of Fig. 4 show the distribution of $|\Delta x| = |x(\Omega_{ci}t = 50) - x(\Omega_{ci}t = 25)|$ for the 750 most energetic particles in each simulation (the choice of $\Omega_{ci}t = 25$ as the earliest time eliminates free streaming along unreconnected field lines before islands develop). The average displacement of the energetic electrons in the 3D system is nearly an order of magnitude greater than that in the 2D simulation, underscoring a fundamental difference in the particle trajectories of the two systems.

The simulations described in this article show an enhancement of electron acceleration efficiency in a 3D system. This contrasts with a recent study of electron-positron plasma, which found no significant difference in the energy spectra of 2D and 3D simulations [19].

However, this study examined a relativistic regime where the reconnection outflow velocity approaches c . A relativistic reconnection outflow inhibits upstream motion of the energetic particles, preventing them from returning to the exhaust region or passing between islands. Another possible reason for the disparity is that simulations in [19] were performed with no asymptotic guide field; the guide field plays an important role in enabling particles to explore the field variations in the z -direction and hence wander in x and y [27].

It has been shown previously that the development of pressure anisotropy with $p_{\parallel} \gg p_{\perp}$ causes the cores of magnetic islands to approach firehose marginal stability, where the tension driving magnetic reconnection ceases, thereby throttling reconnection. A full treatment of the feedback from particle acceleration (e.g. [17]) is outside the scope of this paper. However, we do find that large anisotropies $p_{\parallel} > p_{\perp}$ persist in the 3D simulation, so the turbulent dynamics do not appear to significantly isotropize the pressure. It therefore seems likely that energetic particle feedback on reconnection through the firehose mechanism will continue in the more complex magnetic geometry of 3D systems.

The electron spectra in both simulations do not assume a power law form as is frequently observed in nature. This is due in part to the limited energy gain possible in the modest-sized 3D simulation presented here. Previous 2D simulations have shown the total energy gain is greater in larger systems [18]. An additional issue is that these simulations have periodic boundary conditions so no particles are lost from the system. It has been suggested that the development of a power law requires a loss mechanism in addition to an energy drive [17]. However, recent electron-positron simulations [19, 25] suggest that power laws spectra may still develop in the absence of a loss mechanism. The set of conditions under which power law spectra form in kinetic reconnection simulations remains an open issue.

This work has been supported by NSF Grants AGS1202330 and PHY1102479, and NASA grants NNX11AQ93H, APL-975268, NNX08AV87G, NAS 5- 98033, and NNX08AO83G. Simulations were carried out at the National Energy Research Scientific Computing Center.

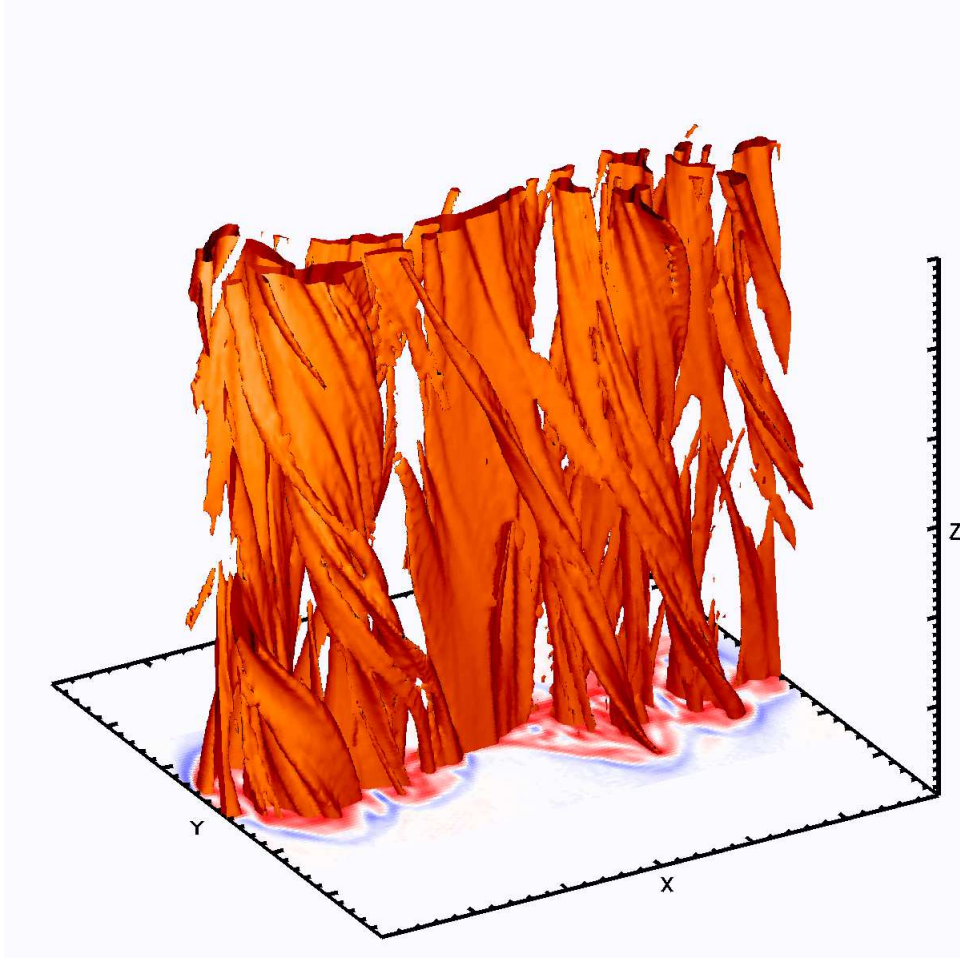


FIG. 1. Isosurface of J_{ez} at $t\Omega_{ci} = 50$. The isosurface level is 60% of the maximum current density (a 2D slice of the same quantity is shown on the bottom). The current is filamentary, exhibiting significant 3D structure.

* Department of Physics, University of Maryland, College Park, Maryland 20742, USA; Institute for Physical Science and Technology, University of Maryland, College Park, Maryland 20742, USA; Space Science Laboratory, University of California, Berkeley, California 94720, USA

[1] G. Drenkhahn and H. C. Spruit, *Astronomy & Astrophysics* **391**, 1141 (2002).

[2] F. C. Michel, *Ap. J.* **431**, 397 (1994).

[3] R. P. Lin, S. Krucker, G. J. Hurford, D. M. Smith, H. S. Hudson, G. D. Holman, R. A. Schwartz, B. R. Dennis, G. H. Share, R. J. Murphy, A. G. Emslie, C. Johns-Krull, and N. Vilmer, *Ap. J.* **595**, L69 (2003).

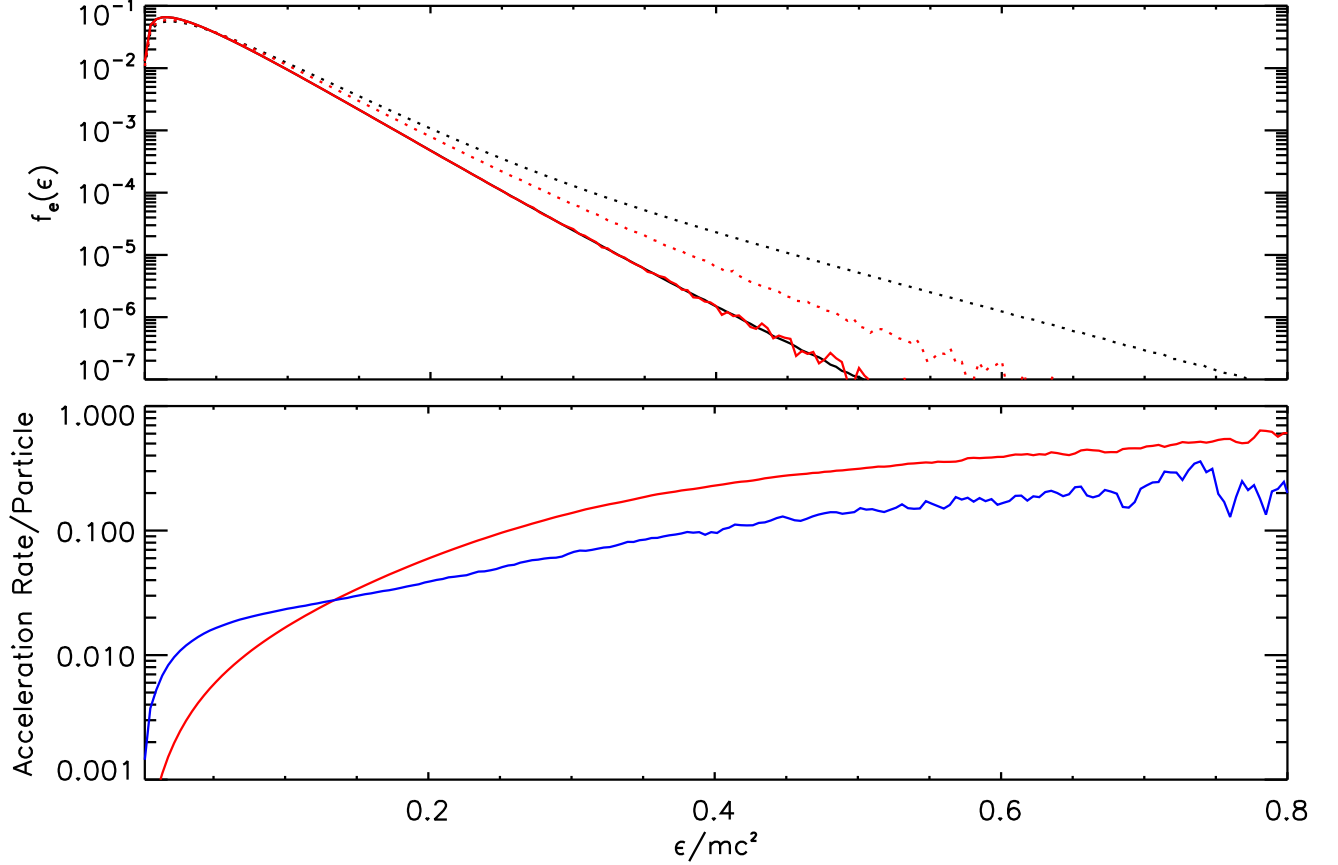


FIG. 2. [Top] Electron energy spectra at the beginning (solid lines) and end (dotted lines) of 2D (red) and 3D (black) simulations. The energetic electrons in the 3D simulation gain significantly more energy. [Bottom] Acceleration due to E_{\parallel} (blue) and Fermi Reflection (red) in the 3D simulation at $t\Omega_{ci} = 50$. Parallel electric fields are most important for low energies, whereas Fermi reflection dominates at high energies.

- [4] M. Øieroset, R. P. Lin, T. D. Phan, D. E. Larson, and S. D. Bale, *Phys. Rev. Lett.* **89**, 195001 (2002).
- [5] S. Krucker, H. S. Hudson, L. Glesener, S. M. White, S. Masuda, J.-P. Wuelser, and R. P. Lin, *Ap. J.* **714**, 1108 (2010).
- [6] M. Oka, S. Ishikawa, P. Saint-Hilaire, S. Krucker, and R. P. Lin, *The Astrophysical Journal* **764**, 6 (2013).
- [7] M. Hoshino, T. Mukai, T. Terasawa, and I. Shinohara, *J. Geophys. Res.* **106**, 25,979 (2001).
- [8] S. Zenitani and M. Hoshino, *Ap. J. Lett.* **562**, L63 (2001).
- [9] J. F. Drake, M. A. Shay, W. Thongthai, and M. Swisdak, *Phys. Rev. Lett.* **94**, 095001 (2005).

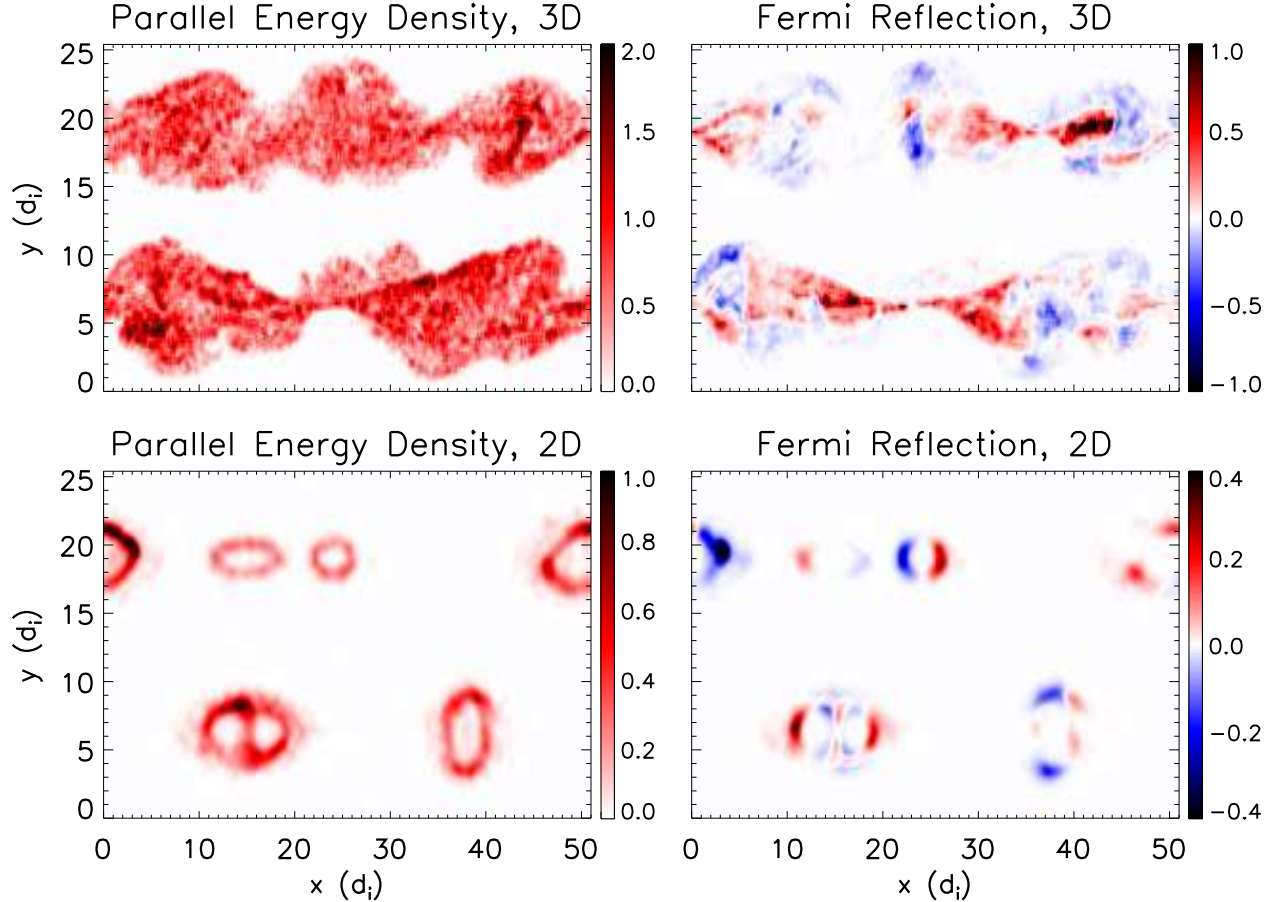


FIG. 3. Parallel energy density and Fermi reflection heating rate for electrons with $\epsilon > 0.5m_e c^2$. The energetic particles are confined to narrow rings in the 2D simulation, but are distributed throughout the reconnecting volume in the 3D simulation. This is reflected in the Fermi reflection heating rate, which is also localized to the rings in the 2D simulation, but distributed throughout the reconnection exhaust in the 3D simulation.

- [10] P. L. Pritchett, *J. Geophys. Res.* **111**, A10212 (2006), 10.1029/2006JA011793.
- [11] J. Egedal, W. Daughton, J. F. Drake, N. Katz, and A. Lê, *Phys. Plasmas* **16**, 050701 (2009), 10.1063/1.3130732.
- [12] M. Oka, T.-D. Phan, S. Krucker, M. Fujimoto, and I. Shinohara, *Ap. J.* **714**, 915 (2010).
- [13] Y. E. Litvinenko, *Ap. J.* **462**, 997 (1996).
- [14] J. Egedal, W. Daughton, and A. Lê, *Nature Phys.* **8**, 321 (2012).
- [15] J. F. Drake, M. Swisdak, H. Che, and M. A. Shay, *Nature* **443**, 553 (2006).
- [16] J. F. Drake, M. Opher, M. Swisdak, and J. N. Chamoun, *Ap. J.* **709**, 963 (2010).
- [17] J. F. Drake, M. Swisdak, and R. Fermo, *The Astrophysical Journal Letters* **763**, L5 (2013).

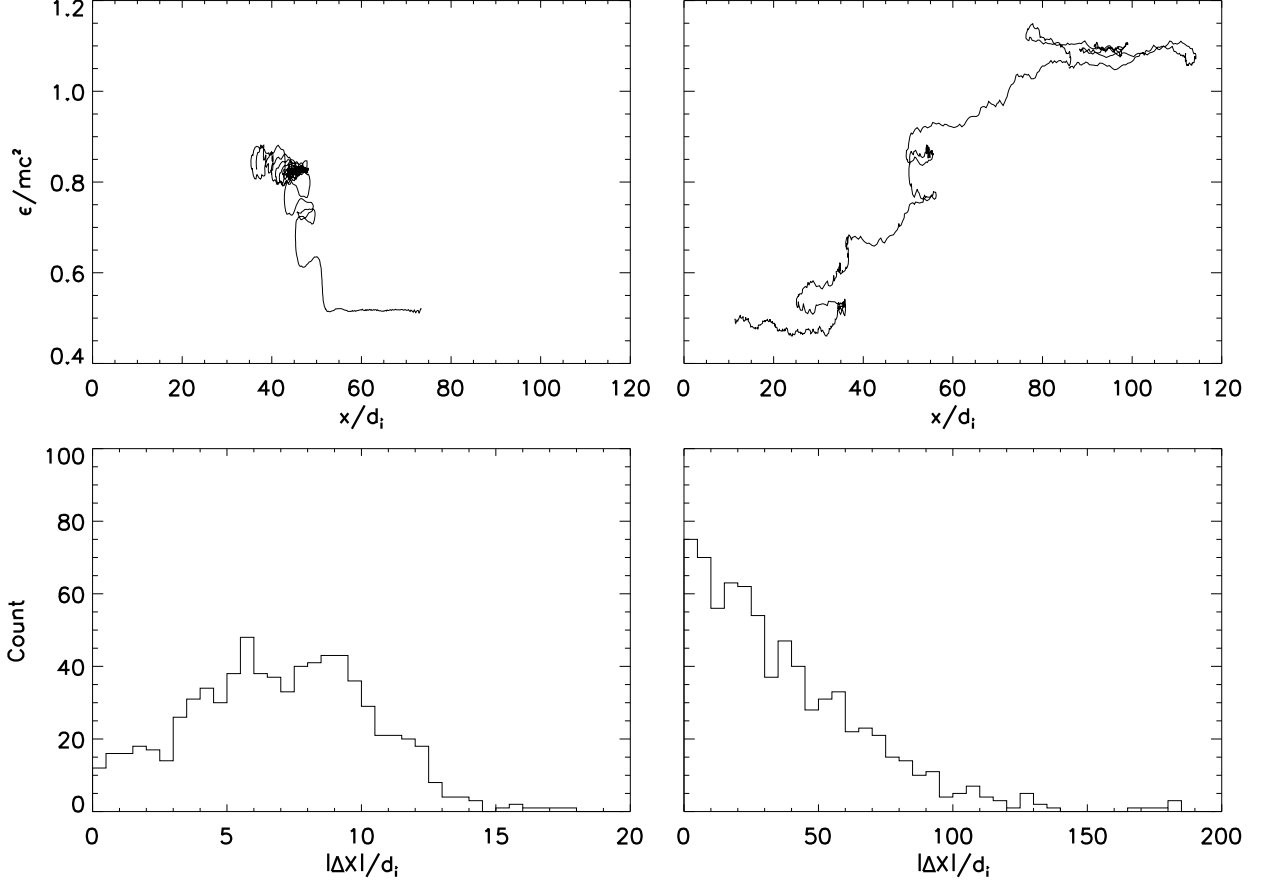


FIG. 4. [Top] Sample trajectories for an energetic particle in the 2D system (left) and the 3D system (right). The electron in the 3D simulation continuously gains energy as it moves throughout the domain. The electron in the 2D simulation is trapped in an island at $x \sim 40$ for a significant period of time and no longer gains energy after the island has released its tension. [Bottom] Distribution of $\Delta X = |x(t=50) - x(t=25)|$ for the 750 most energetic particles in the 2D simulation (left) and 3D simulation (right). The particles in the 3D simulation are able to access a much larger fraction of the simulation domain.

- [18] J. T. Dahlin, J. F. Drake, and M. Swisdak, *Physics of Plasmas* (1994-present) **21**, 092304 (2014).
- [19] F. Guo, H. Li, W. Daughton, and Y.-H. Liu, *Phys. Rev. Lett.* **113**, 155005 (2014).
- [20] P. L. Pritchett, *J. Geophys. Res.* **113**, A06210 (2008), 10.1029/2007JA012930.
- [21] R. Schreier, M. Swisdak, J. F. Drake, and P. A. Cassak, *Phys. Plasmas* **17**, 110704 (2010), 10.1063/1.3494218.
- [22] W. Daughton, V. Roytershteyn, H. Karimabadi, L. Yin, B. J. Albright, B. Bergen, and K. J. Bowers, *Nature Phys.* **7**, 539 (2011).

- [23] M. Onofri, H. Isliker, and L. Vlahos, *Phys. Rev. Lett.* **96**, 151102 (2006), 10.1103/PhysRevLett96.151102.
- [24] G. Kowal, E. M. de Gouveia Dal Pino, and A. Lazarian, *The Astrophysical Journal* **735**, 102 (2011).
- [25] L. Sironi and A. Spitkovsky, *The Astrophysical Journal Letters* **783**, L21 (2014).
- [26] A. Zeiler, D. Biskamp, J. F. Drake, B. N. Rogers, M. A. Shay, and M. Scholer, *J. Geophys. Res.* **107**, 1230 (2002).
- [27] J. R. Jokipii and E. N. Parker, *Astrophys. J.* **155**, 777 (1969).
- [28] T. G. Northrop, “The adiabatic motion of charged particles,” (Interscience Publishers, 1963).
- [29] See Supplemental Material at [URL] for .mov movies of the particle trajectories.